

# Pre-training Tensor-Train Networks Facilitates Machine Learning with Variational Quantum Circuits

Jun Qi<sup>1,4</sup>, Chao-Han Yang<sup>1,2</sup>, Pin-Yu Chen<sup>3</sup>, Min-Hsiu Hsieh<sup>5</sup>

1. Electrical and Computer Engineering, Georgia Institute of Technology, Atlanta, GA 30332, USA
2. NVIDIA Research, Santa Clara, CA 95051, USA
3. IBM Research, Yorktown Heights, NY 10598, USA
4. Computer Science, Hong Kong Baptist University, Hong Kong
5. Hon Hai Quantum Computing Research Center, Taipei, Taiwan

**Abstract.** Variational quantum circuits (VQCs) hold promise for quantum machine learning on noisy intermediate-scale quantum (NISQ) devices. While tensor-train networks (TTNs) can enhance VQC representation and generalization, the resulting hybrid model, TTN-VQC, faces optimization challenges due to the Polyak-Lojasiewicz (PL) condition. To mitigate this challenge, we introduce Pre+TTN-VQC, a pre-trained TTN model combined with a VQC. Our theoretical analysis, grounded in two-stage empirical risk minimization, provides an upper bound on the transfer learning risk. It demonstrates the approach’s advantages in overcoming the optimization challenge while maintaining TTN-VQC’s generalization capability. We validate our findings through experiments on quantum dot and handwritten digit classification using simulated and actual NISQ environments.

## 1. INTRODUCTION

Quantum machine learning (QML) is an interdisciplinary field that integrates quantum computing and machine learning [1–5]. With the rapid development of near-term quantum computers, we have witnessed the noisy intermediate-scale quantum (NISQ) devices that admit as many as a few hundred qubits available for implementing many QML algorithms on actual quantum computers to enhance the computational efficiency of machine learning applications [6–8]. Since NISQ devices are characterized by a few qubits and high levels of quantum noise, we are exploring the potential of classical machine learning to scale up QML algorithms in use cases [9–11]. For example, variational quantum circuits (VQC) with adjustable parameters can constitute quantum neural networks (QNN) for processing data and making predictions [12–16]. Since VQC is resilient to the quantum noise on NISQ devices, VQC consists of parametric quantum circuits optimized via stochastic gradient descent (SGD) to minimize the cost function in a back-propagation manner [17, 18].

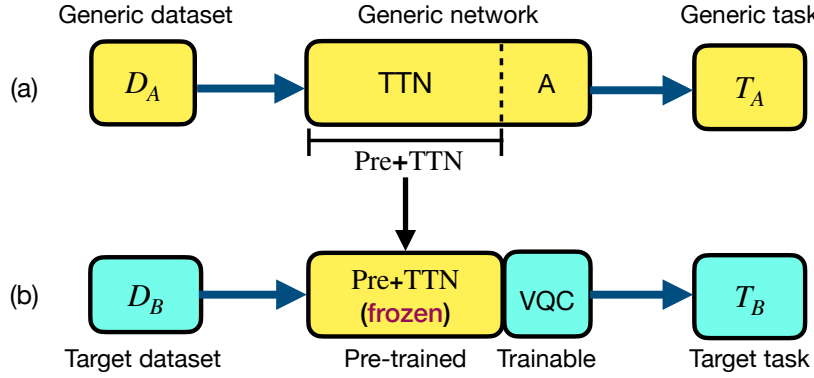


**Figure 1. A demonstration of learning paradigm for Pre+TTN-VQC.** (a) An illustration of a generic TTN-VQC trained on the source dataset  $D_A$  for the target task  $T_A$ ; (b) The pre-trained TTN is transferred to TTN-VQC constituting a Pre+TTN-VQC model, where the Pre+TTN is frozen, and the VQC model needs a further adjustment on the target dataset  $D_B$  for target task  $T_B$ .

However, ensuring VQC’s optimization performance is a critical challenge in QML on NISQ devices. NISQ devices suffer from high levels of noise that can disrupt the optimization process [19]. This noise can lead the optimizer, like SGD, to converge to suboptimal solutions. Particularly, simulating large quantum circuits quickly becomes intractable with increasing qubits due to the exponential growth in complexity. Our previous work [20] demonstrated that a tensor-train network (TTN) [21, 22] could improve VQC’s representation and generalization powers, admitting an end-to-end quantum learning paradigm. Still, the hybrid quantum-classical model TTN-VQC, combining TTN with VQC in an end-to-end learning paradigm [23], requires a Polyak-Lojasiewicz (PL) condition [24] to satisfy optimization performance with exponential convergence rates. However, the PL condition for TTN-VQC is sufficient but not necessary to guarantee the VQC’s optimization performance, and the PL condition is only easily realized on some machine learning datasets.

Thus, this work is devoted to exploiting a pre-training strategy for TTN, namely Pre+TTN, before combining it with VQC to generate Pre+TTN-VQC. The pre-training approach has been widely adopted in deep learning technologies [25–27] and incredibly generative artificial intelligence like large language models [28, 29]. Figure 1 demonstrates the learning paradigm of Pre+TTN-VQC with a pre-trained TTN and a VQC classifier for making predictions. The pre-trained TTN refers to a classical model whose parameters do not participate in the VQC fine-tuning process, and the VQC model’s parameters need further adjustment based on the target dataset  $D_B$ . Our hybrid quantum-classical architecture balances the powers of the classical tensor network approach and the quantum advantages offered by the VQC. The pre-trained TTN reduces data dimensionality and enhances the VQC’s generalization performance by reducing classical-to-quantum transfer learning risk. Our theoretical and empirical contributions are summarized below:

- (i) We modify our end-to-end quantum learning paradigm based on TTN-VQC using a pre-trained TTN, where the classical TTN is pre-trained and frozen before combining it with the VQC.
- (ii) We demonstrate that the pre-trained TTN can improve the VQC's generalization power by reducing the transfer learning risk associated with our hybrid quantum-classical architecture as illustrated in Figure 1.
- (iii) We corroborate our theoretical results by showing our experiments of semiconductor quantum dot prediction and handwritten digit classification. The experiments of quantum dot prediction are associated with quantum data, while handwritten digit classification refers to a classical task.

Compared to a similar pre-training matrix product state work for quantum machine learning [30], our proposed pre-training approach of TTN is built upon a transfer learning architecture [31] and mainly focuses on improving VQC's generalization power via reducing the transfer learning risk. Moreover, we demonstrate that the pre-trained TTN for VQC can outperform our previously proposed end-to-end quantum learning approach based on TTN-VQC [20] in terms of higher accuracy and less training data required for VQC. Besides, the Pre+TTN-VQC model shares the same sample complexity as VQC in the training process but significantly attains much better empirical performance than VQC.

## 2. PRELIMINARIES

### 2.1. Variational Quantum Circuits

In the NISQ era, a quantum neural network (QNN) relies on the variational quantum circuits (VQC) architecture. As shown in Figure 2, the VQC model consists of three components: (a) Quantum Data Encoding, (b) Parametric Quantum Circuits (PQC), and (c) Quantum Measurement.

Angle and amplitude encoding are two quantum data encoding schemes, and in this work, we consider angle encoding based on tensor product encoding (TPE). The TPE employs a series of  $R_Y(\frac{\pi}{2}x_i)$  to generate a quantum state  $|\mathbf{x}\rangle$  from a classical vector  $\mathbf{x}$  by adopting a one-to-one mapping as given in Eq. (1).

$$\begin{aligned}
 |\mathbf{x}\rangle &= \left( \otimes_{i=1}^U R_Y \left( \frac{\pi}{2} \phi(x_i) \right) \right) |0\rangle^{\otimes U} \\
 &= \begin{bmatrix} \cos(\frac{\pi}{2}\phi(x_1)) \\ \sin(\frac{\pi}{2}\phi(x_1)) \end{bmatrix} \otimes \begin{bmatrix} \cos(\frac{\pi}{2}\phi(x_2)) \\ \sin(\frac{\pi}{2}\phi(x_2)) \end{bmatrix} \otimes \cdots \otimes \begin{bmatrix} \cos(\frac{\pi}{2}\phi(x_U)) \\ \sin(\frac{\pi}{2}\phi(x_U)) \end{bmatrix},
 \end{aligned} \tag{1}$$

where  $U$  stands for the number of qubits, and  $x_i$  refers to the  $i^{th}$  component in the vector  $\mathbf{x}$ . Eq. (1) suggests that a  $2^U$ -dimensional quantum state  $|\mathbf{x}\rangle$  can be represented as the tensor product of  $U$  2-dimensional vectors associated with classical data  $x_i$ , and the sigmoid function  $\phi(x_i)$  constrains the value domain of  $\phi(x_i) \in [0, 1]$ .

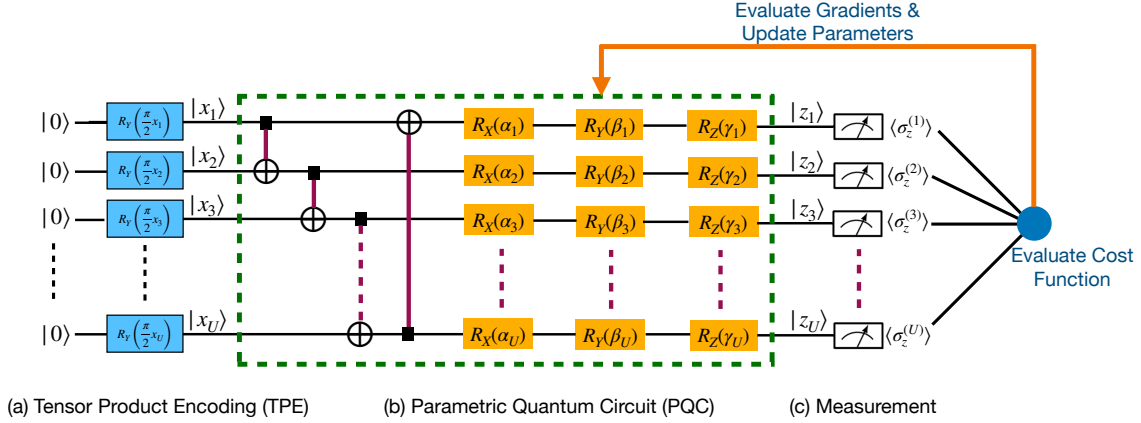


**Figure 2. The components of the VQC model:** (a) Quantum Data Encoding based on Tensor Product Encoding (TPE); (b) Parametric Quantum Circuits (PQC); (c) Measurement.

The PQC framework comprises the component of quantum entanglement using controlled-not (CNOT) gates and build the parametric models based on Pauli rotation gates  $R_X$ ,  $R_Y$  and  $R_Z$  with adjustable parameters  $\alpha = \{\alpha_1, \alpha_2, \dots, \alpha_U\}$ ,  $\beta = \{\beta_1, \beta_2, \dots, \beta_U\}$ , and  $\gamma = \{\gamma_1, \gamma_2, \dots, \gamma_U\}$ . The PQC is associated with a linear operator that transforms the quantum input state  $|\mathbf{x}\rangle$  into the output  $|\mathbf{z}\rangle$ . The PQC in the green dashed square is repeatedly copied to create a deep structure.

The measurement component outputs a series of expected observations based on the Hermitian operators  $\sigma_z^{(1)}$ ,  $\sigma_z^{(2)}$ , ...,  $\sigma_z^{(U)}$ , by converting the quantum states  $|z_1\rangle$ ,  $|z_2\rangle$ , ...,  $|z_U\rangle$  into the corresponding expectation values  $\langle\sigma_z^{(1)}\rangle$ ,  $\langle\sigma_z^{(2)}\rangle$ , ...,  $\langle\sigma_z^{(U)}\rangle$ , which are connected to a final softmax function to calculate the loss value. For the experimental simulation on a classical GPU/GPU, a back-propagation approach based on stochastic gradient descent (SGD) optimizer is utilized to update the PQC parameters. However, if we run our experiments on a real quantum computer, the parameter-shift rule approximates the first-order gradients to adjust the model parameters.

## 2.2. Tensor-Train Networks

A tensor-train network (TTN), or matrix product state (MPS), is a particular type of neural network that excels in handling high-dimensional data while efficiently managing memory and computational resources. TTN represents high-dimensional tensors (multi-dimensional arrays) as a chain of smaller, three-index tensors. More specifically, for an integer  $I = \prod_{k=1}^K I_k$ , a vector  $\mathbf{x} \in \mathbb{R}^I$  can be reshaped into a  $K$ -order tensor  $\mathcal{X} \in \mathbb{R}^{I_1 \times I_2 \times \dots \times I_{K+1}}$ . Then, given the tensor-train ranks (TT-ranks) as  $\{r_1, r_2, \dots, r_K\}$ , where  $r_1$  and  $r_{K+1}$  are set to 1, all elements of  $\mathcal{X}$  are represented by multiplying  $K$  matrices  $\mathcal{X}_k(i_k)$  based on the TT formats, as shown in Eq. (2).

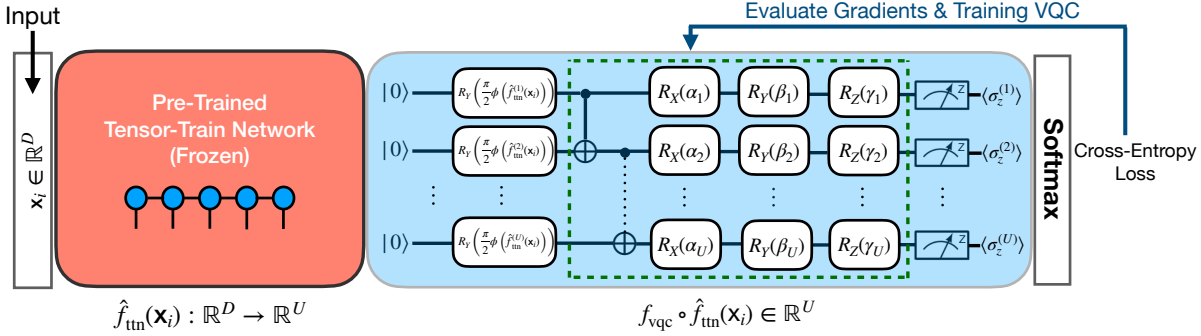


Figure 3. An illustration of the Pre-TTN+VQC architecture.

$$\mathcal{X}(i_1, i_2, \dots, i_K) = \prod_{k=1}^K \mathcal{X}_k(i_k), \quad (2)$$

where the matrices  $\mathcal{X}(i_k) \in \mathbb{R}^{r_k \times r_{k+1}}$ ,  $\forall i_k \in [I_k]$ .

Besides, we can use the TT format to represent a 2-dimensional matrix. In more detail, we can reshape a matrix  $\mathbb{W}$  as a  $K$ -order double indexed tensor  $\mathcal{W}$ , as given in Eq. (3).

$$\mathcal{W}((i_1, j_1), (i_2, j_2), \dots, (i_K, j_K)) = \prod_{k=1}^K \mathcal{W}_k(i_k, j_k), \quad (3)$$

where  $\mathcal{W}_k \in \mathbb{R}^{r_k \times I_k \times J_k \times r_{k+1}}$  is a 4-order tensor, and each element  $\mathcal{W}_k(i_k, j_k) \in \mathbb{R}^{r_k \times r_{k+1}}$  refers to a matrix. Then, a TTN can output a  $K$ -order tensor  $\mathcal{Y}$  from a  $K$ -order input tensor  $\mathcal{X}$  by applying Eq. (4).

$$\mathcal{Y}(j_1, j_2, \dots, j_K) = \prod_{k=1}^K \sum_{i_k=1}^{I_k} \mathcal{W}_k(i_k, j_k) \odot \mathcal{X}_k(i_k) = \prod_{k=1}^K \mathcal{Y}_k(j_k), \quad (4)$$

where  $\mathcal{W}_k(i_k, j_k) \odot \mathcal{X}_k(i_k)$  denotes an element-wise multiplication of the two matrices, and thus  $\sum_{i_k=1}^{I_k} \mathcal{W}_k(i_k, j_k) \odot \mathcal{X}_k(i_k)$  results in a new matrix  $\mathcal{Y}_k(j_k) \in \mathbb{R}^{r_k \times r_{k+1}}$ . Moreover, we set the ranks  $r_1 = r_{K+1} = 1$  to make  $\prod_{k=1}^K \mathcal{Y}_k(j_k)$  become a scalar.

Besides, the TTN is a classical simulation of quantum circuits, and it can be implemented using universal quantum gates on real quantum computers. The combination of TTN and VQC, namely TTN-VQC, can potentially be taken as an end-to-end quantum learning paradigm [32]. Moreover, TTN enables a compact TT-format tensor representation for high-dimensional features, particularly for angle encoding in VQC [22, 33].

### 3. RESULTS

#### 3.1. Theoretical results

Based on the end-to-end quantum learning paradigm based on TTN-VQC [20, 32], we put forth a Pre+TTN-VQC pipeline as shown in Figure 3. A pre-trained TTN operator  $\hat{f}_{\text{ttn}}$  transforms high-dimensional input data  $\mathbf{x}_i \in \mathbb{R}^D$  into a low-dimensional features  $\mathbf{x}_i \in \mathbb{R}^U$ , where  $U$  corresponds to the number of quantum channels in VQC. In the Pre+TTN-VQC architecture, a series of Pauli-Y gates  $R_Y$  encodes the classical value  $\mathbf{x}_i$  into the quantum states  $R_Y(\frac{\pi}{2}\phi(\hat{f}_{\text{ttn}}^{(j)}(\mathbf{x}_i)))$  of the  $j^{\text{th}}$  quantum channel. In particular, we use a sigmoid function  $\phi(\cdot)$  to constrain the values of  $\hat{f}_{\text{ttn}}^{(j)}(\mathbf{x}_i)$  in the domain of  $(0, 1)$ . The parametric quantum gates (PQC) consist of Pauli rotation gates  $R_X(\alpha_j)$ ,  $R_Y(\beta_j)$  and  $R_Z(\gamma_j)$  whose parameters  $\alpha_j$ ,  $\beta_j$  and  $\gamma_j$  need adjustable during the VQC training process. The pre-trained VQC does not participate in the VQC fine-tuning process, which means its parameters are frozen without further adjustment. The quantum states associated with the PQC's outputs are then converted back to classical data via the quantum measurement, which results in the expected values  $\langle \sigma_z^{(j)} \rangle$ . The VQC's outputs  $\langle \sigma_z^{(j)} \rangle$  are connected to the softmax operation with the cross-entropy loss function [34]. The loss function's gradients are returned to update the VQC's parameters.

As for the theoretical analysis of Pre-TTN+VQC, we consider a two-stage empirical risk minimization (ERM) [35] procedure, where we define the TTN, classical model A, and VQC operators as  $f_{\text{ttn}} \in \mathbb{F}_{\text{TTN}}$ ,  $f_a \in \mathbb{F}_A$ , and  $f_{\text{vqc}} \in \mathbb{F}_{\text{VQC}}$ , respectively. In the first stage, we aim to pre-train a TTN model on the source dataset; in the second phase, we transfer the pre-trained TTN model to the hybrid quantum-classical model and update the VQC's parameters on the target dataset.

In the first training phase, the classical end-to-end model TTN+A is pre-trained from the source dataset  $S_0$ , and the empirical risk of TTN+A is defined as Eq. (5).

$$\hat{R}_{\text{tr1}}(f_a, f_{\text{ttn}}) := \frac{1}{|S_0|} \sum_{n=1}^{|S_0|} \ell(f_a \circ f_{\text{ttn}}(\mathbf{x}_n), y_n), \quad (5)$$

where  $\ell$  is the loss function,  $\mathbf{x}_n$  denotes the feature vector, and  $y_n$  is the label corresponding to  $\mathbf{x}_n$ . The pre-trained TTN is denoted by  $\hat{f}_{\text{ttn}}$  as given in Eq. (6).

$$\hat{f}_{\text{ttn}} = \arg \min_{f_{\text{ttn}} \in \mathbb{F}_{\text{TTN}}} \min_{f_a \in \mathbb{F}_A} \hat{R}_{\text{tr1}}(f_a, f_{\text{ttn}}). \quad (6)$$

For the second training stage, which employs the quantum approach, the empirical risk for the training on the target dataset  $S_T$  is given by Eq. (7).

$$\hat{R}_{\text{tr2}}(f_{\text{vqc}}, \hat{f}_{\text{ttn}}) := \frac{1}{|S_T|} \sum_{m=1}^{|S_T|} \ell(f_{\text{vqc}} \circ \hat{f}_{\text{ttn}}(\mathbf{x}_m), y_m). \quad (7)$$

Moreover, we estimate the underlying function  $\hat{f}_{\text{ttn}}$  for the target dataset  $S_T$  by computing the ERM based on the  $\hat{f}_{\text{ttn}}$  learned in the first phase, as given in Eq. (8).

$$\hat{f}_{\text{vqc}} := \arg \min_{f_{\text{vqc}} \in \mathbb{F}_{\text{VQC}}} \hat{R}_{\text{tr}_2}(f_{\text{vqc}}, \hat{f}_{\text{ttn}}). \quad (8)$$

Then, we define the transfer learning risk  $R_{\text{tl}}$  as given in Eq. (9).

$$R_{\text{tl}} = R_{\text{tr}_2}(\hat{f}_{\text{vqc}}, \hat{f}_{\text{ttn}}) - R_{\text{tr}_2}(f_{\text{vqc}}^*, f_{\text{ttn}}^*), \quad (9)$$

where  $R_{\text{tr}_2}(\cdot, \cdot) = \mathbb{E}[\hat{R}_{\text{tr}_2}(\cdot, \cdot)]$  refers to the population risk for the target dataset.  $f_{\text{ttn}}^*$  and  $f_{\text{vqc}}^*$  separately denote the optimal TTN and VQC operators. The transfer learning risk  $R_{\text{tl}}$  measures the expected prediction risk  $R_{\text{tr}_2}(\hat{f}_{\text{vqc}}, \hat{f}_{\text{ttn}})$  on the target dataset  $S_T$ , relative to the best prediction rule from which the data are generated from the optimal TTN-VQC operator  $f_{\text{vqc}}^* \circ f_{\text{ttn}}^*$ .

Furthermore, given the measurement of model complexity  $\mathcal{C}$ , we can upper bound the transfer learning risk  $R_{\text{tl}}$  as Eq. (10).

$$R_{\text{tl}} = \tilde{\mathcal{O}} \left( \frac{1}{\nu} \left( \sqrt{\frac{\mathcal{C}(\mathbb{F}_{\text{TTN}}) + \mathcal{C}(\mathbb{F}_A)}{|S_0|}} \right) + \sqrt{\frac{\mathcal{C}(\mathbb{F}_{\text{VQC}})}{|S_T|}} \right), \quad (10)$$

where  $\nu$  is a constant related to the task-agnostic notion of task diversity, and  $\mathcal{C}(\cdot)$  measures the intrinsic complexity of the functional class. Thus,  $\mathcal{C}(\mathbb{F}_{\text{TTN}})$  captures the complexity of the pre-trained TTN, and  $\mathcal{C}(\mathbb{F}_{\text{VQC}})$  correspond to the model complexity of VQC.

Besides, when the source data are abundant, obtaining a fixed level of constant prediction errors on the target dataset only requires the number of fresh samples to be  $|S_T| \approx \mathcal{C}(\mathbb{F}_{\text{VQC}})$ . On the other hand, learning the task in isolation suffers the burden of learning both  $\mathbb{F}_{\text{VQC}}$  and  $\mathbb{F}_{\text{TTN}}$ , which is  $|S_T| \approx \mathcal{C}(\mathbb{F}_{\text{TTN}}) + \mathcal{C}(\mathbb{F}_{\text{VQC}})$ , therefore much greater than the transfer learning sample complexity. Most importantly, our derived upper bound in Eq. (9) suggests that the transfer learning risk can be lowered down to a small value by scaling the source data  $S_0$  and the target dataset  $S_T$ , where we do not rely on the PL condition used for the setup of TTN-VQC.

To corroborate the approach of using pre-trained TTN for VQC, we compare Pre-TTN+VQC with TTN+VQC and VQC counterparts on both quantum and classical data use cases. The datasets comprise a source dataset  $S_0$  for training the TTN model and a target dataset  $S_T$  for fine-tuning the VQC, where there is no overlapping between  $S_0$  and  $S_T$ . The test data share the same classified labels as the target ones but are omitted in  $S_T$ . Our experimental results compare the performance of Pre+TTN-VQC with the baseline results of the TTN-VQC and VQC counterparts discussed in [20, 32].

### 3.2. Empirical results of handwritten digit classification

First, we assess the performance of Pre+TTN-VQC on the classical MNIST dataset [36]. The dataset focuses on handwritten ten-digit classification, where 60,000 training data and 10,000 test data are included. We randomly collect 18,000 training data of six digits  $\{1, 2, 3, 4, 5, 6\}$  to include in the source dataset  $S_0$  and assign another 2,000 training data

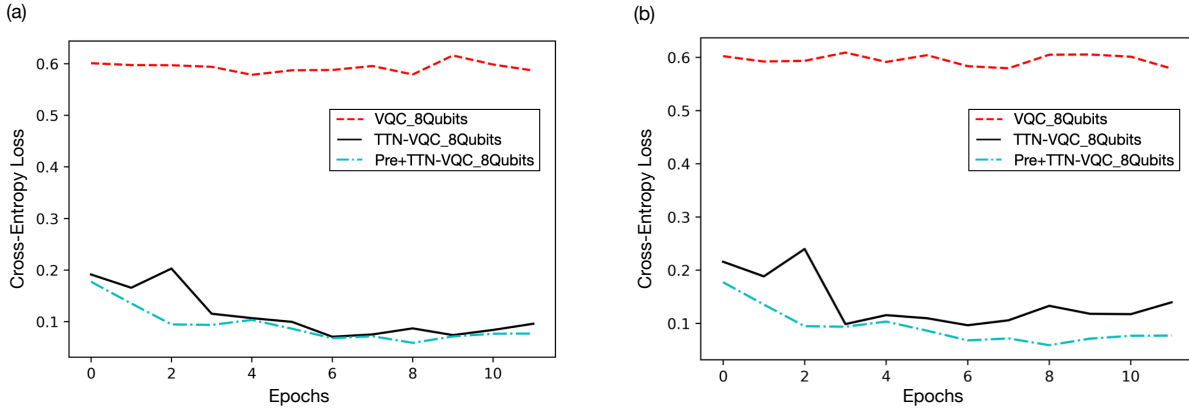


**Figure 4. Experimental results on the MNIST dataset to assess the empirical performance of Pre+TTN-VQC.** (a) Empirical results on the training data. (b) Empirical results on the test data. VQC\_8Qubit represents the VQC model with 8 qubits; TTN-VQC\_8Qubits and Pre+TTN-VQC\_8Qubits separately stand for the TTN-VQC and Pre+TTN-VQC models with 8 qubits.

of two digits  $\{2, 5\}$  to constitute the target dataset  $S_T$ . Accordingly, the test dataset comprises all the test data of digits  $\{2, 5\}$ , which are not seen in the dataset  $S_0$  and  $S_T$ .

As for the setup of Pre+TTN-VQC and TTN-VQC, the image data are reshaped into 3-order  $7 \times 16 \times 7$  tensors. Given the TT-ranks  $\{1, 3, 3, 1\}$ , we set three trainable tensors:  $\mathcal{W}_1 \in \mathbb{R}^{1 \times 7 \times U_1 \times 3}$ ,  $\mathcal{W}_2 \in \mathbb{R}^{3 \times 16 \times U_2 \times 3}$ , and  $\mathcal{W}_3 \in \mathbb{R}^{3 \times 7 \times U_3 \times 1}$ , where  $U = \prod_{k=1}^3 U_k$  stands for the number of qubits. In particular, we evaluate the models with 8 qubits, and the hyper-parameters  $(U_1, U_2, U_3)$  are set as  $(2, 2, 2)$  to match with the number of qubits used in our experiments. The SGD algorithm with an Adam optimizer is employed in the training process, where the cross-entropy (CE) is chosen as the loss function, and a mini-batch of 50 and a learning rate of 0.001 are configured in the training process. Besides, we compare the Pre+TTN-VQC with the baseline models of TTN-VQC and VQC. The TTN-VQC follows an end-to-end learning paradigm, while the VQC takes principal component analysis (PCA) for the feature dimensionality. The training data subsets  $S_0$  and  $S_T$  jointly train both VQC and TTN-VQC. We utilize 8 qubits in our experiments to compose the VQC model.

Figure 4 shows empirical results of binary handwritten digit classification. The experimental results show that both TTN-VQC and Pre+TTN-VQC can converge to low CE values, but the VQC model cannot decrease the CE loss on a small scale because of its potential trainability challenge. Moreover, Table 1 presents the final experimental results of the related models on the test dataset. Both Pre+TTN-VQC and TTN-VQC own more parameters than VQC, but the former achieves much lower CE scores and higher accuracies. Moreover, the Pre+TTN-VQC attains better empirical performance than the TTN-VQC with a lower CE score (0.0769 vs. 0.0943) and a higher accuracy (99.0% vs. 98.7%).

Furthermore, we incrementally increase the amount of training data in  $S_0$ , and the related experimental results are shown in Table 2. The results suggest that the

**Table 1.** Empirical results of Pre+TTN-VQC, TTN-VQC, and VQC models on the test dataset to assess their empirical performance on the MNIST dataset

Models	Params (Mb)	CE	Accuracy (%)
VQC_8Qubit	0.080	0.5868	72.5
TTN-VQC_8Qubit	0.452	0.0943	97.8
Pre+TTN-VQC_8Qubit	0.452	0.0769	98.5

empirical performance of Pre+TTN-VQC can become even better with an increase in the amount of source training data in  $S_0$ , which corroborates our theoretical result that a more extensive dataset  $S_0$  correspond to a lower transfer learning risk.

**Table 2.** Empirical results of the Pre+TTN-VQC on the source dataset of different amounts of data in  $S_0$ .

Models	# Data in $S_0$	CE	Accuracy (%)
Pre+TTN-VQC_8Qubit	18,000	0.0390	99.0
Pre+TTN-VQC_8Qubit	24,000	0.0347	99.1
Pre+TTN-VQC_8Qubit	30,000	0.0321	99.3

Besides, we observe the empirical performance by increasing the target data amount in  $S_T$ . The results in Table 3 show that with the increase of the amount of target data in  $S_T$ , the Pre+TTN-VQC can consistently obtain lower CE scores and higher accuracies, which corroborate our theoretical results that more target data in  $S_T$  results in a lower upper bound on the transfer learning risk. In particular, increasing the amount of data in  $S_T$  cannot contribute more gain to the empirical performance compared to the increase of data in  $S_0$ , which means that the pre-training approach plays a more critical role in reducing the transfer learning risk. Besides, the improved experimental performance of Pre+TTN-VQC does not require the PL condition, and the related experiments corroborate our derived upper bound on the transfer learning risk in Eq. (9), demonstrating the effectiveness of the pre-training approach for TTN.

**Table 3.** Empirical results of the Pre+TTN-VQC on the target dataset of different amounts of data in  $S_T$ .

Models	# Data in $S_T$	CE	Accuracy (%)
Pre+TTN-VQC_8Qubit	2,000	0.0769	98.5
Pre+TTN-VQC_8Qubit	2,500	0.0713	98.6
Pre+TTN-VQC_8Qubit	3,000	0.0678	98.8

### 3.3. Empirical results of semiconductor quantum dot classification

We demonstrate the advantage of the pre-trained TTN model for VQC from our semiconductor quantum dot classification experiments, which corresponds to a binary

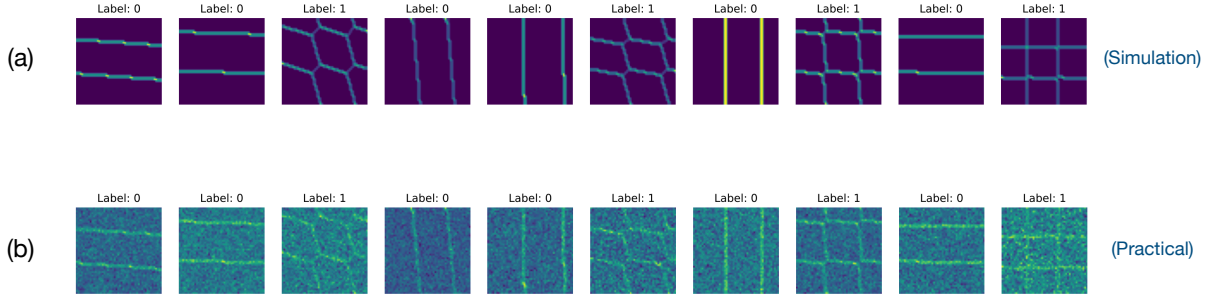


**Figure 5. Illustration of single and double quantum dot charge stability diagrams.** (a) labeled clean charge stability diagrams containing the transition lines without noise; (b) labeled noisy charge stability diagrams mixed with realistic noise effects on the transition lines. Label:0 and Label:1 denote charge stability diagrams of single and double quantum dots.

classification task of single and double quantum dot charge stability diagram [37–39]. As shown in Figure 7, we first simulate clean charge stability diagrams containing transition lines and collect the corresponding experimental diagrams with realistic noisy effects. We separately assess the empirical performance of Pre+TTN-VQC, TTN-VQC, and VQC models on clean and noisy datasets, where each dataset is randomly partitioned into a training dataset with 80% data and a test one with the remaining data. The setups of TTN in the experiments are kept the same as those in our experiments on the MNIST dataset. We utilize the CE as the loss function and employ the Adam optimizer with a learning rate of 0.001 to update the VQC model parameters.

In our experiments, we separately assess the empirical performance of Pre+TTN-VQC on the clean and noisy datasets while comparing it with VQC and TTN-VQC counterparts. For the experiments on the clean dataset, our results show that both TTN-VQC and Pre+TTN-VQC can achieve 100% accuracy, but Pre+TTN-VQC attains a lower loss value than TTN-VQC, while both Pre+TTN-VQC and TTN-VQC significantly outperforms VQC. Regarding our experiments on the noisy dataset, the Pre+TTN-VQC achieves an outstanding performance gain compared to the baseline results of TTN-VQC and VQC in terms of higher accuracy and lower loss scores.

The experimental results show that the Pre+TTN-VQC can achieve even better generalization performance than TTN-VQC, where the PL condition is not necessarily required. This means we can ensure the TTN-VQC's generalization power by reducing the transfer learning risk in Eq. (9), which can further improve the TTN-VQC's empirical results in dealing with quantum machine learning tasks.

#### 4. DISCUSSION

This work introduces a pre-trained approach for TTN to facilitate quantum machine learning with the VQC architecture. The proposed Pre+TTN-VQC is built upon an end-to-end quantum learning paradigm based on TTN-VQC, where TTN is pre-trained

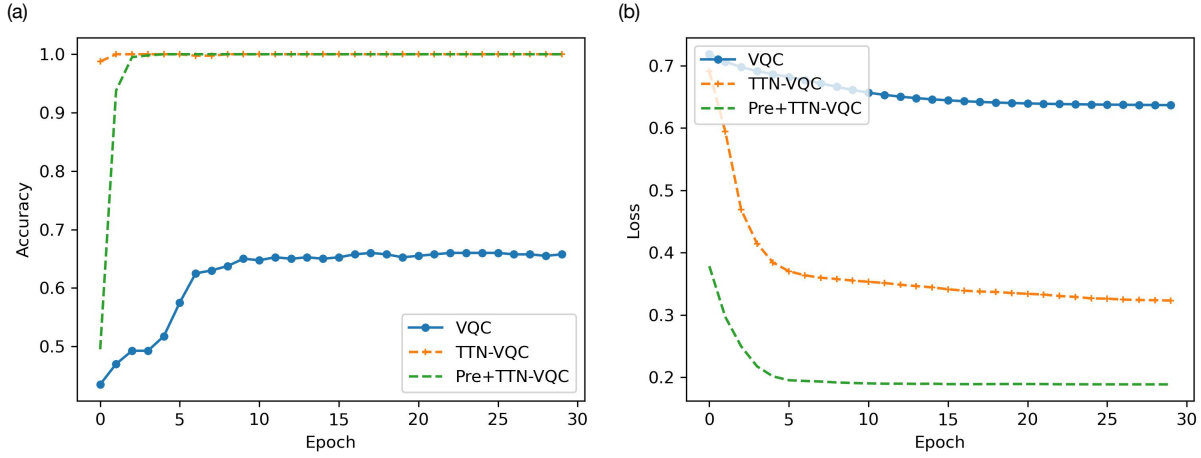


**Figure 6. Experimental results on clean charge stability diagrams with 8 qubits.** (a) The accuracy of our empirical performance; (b) Our experimental results regarding loss scores.

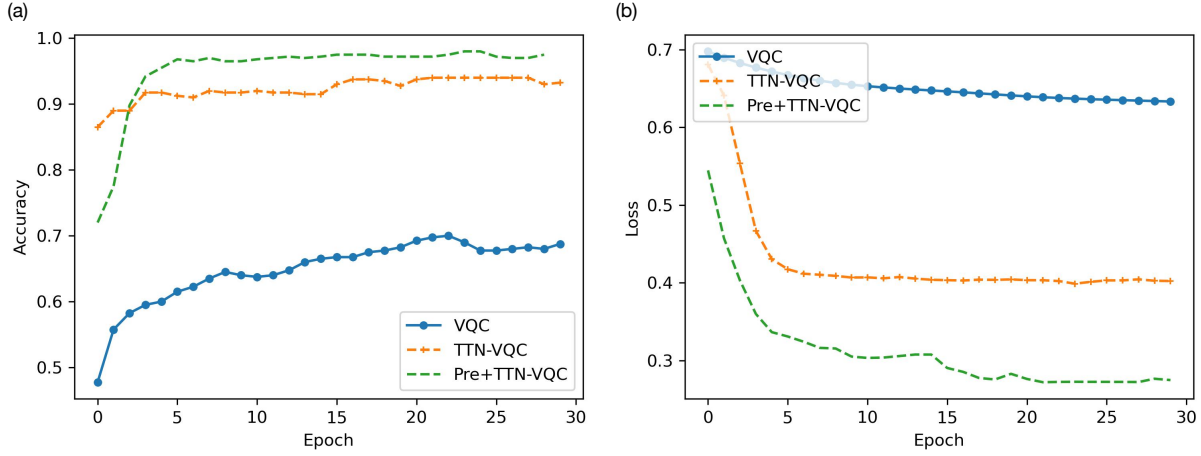


**Figure 7. Experimental results on noisy charge stability diagrams with 8 qubits.** (a) The accuracy of our empirical performance; (b) Our experimental results regarding loss scores.

on a classical machine learning pipeline. Our theoretical understanding suggests that the Pre+TTN-VQC model does not rely on the PL condition to achieve a good optimization performance but requires scaling down the amount of source training data to reduce the transfer learning risk. We employ handwritten digit classification and semiconductor quantum dot prediction tasks to corroborate our theoretical analysis. We observe that our experimental results of both classical and quantum tasks can verify the performance advantages of the Pre+TTN-VQC over the TTN-VQC and VQC counterparts. Most importantly, the improved experimental performance of TTN-VQC does not need the setup of PL condition.

## 5. METHODS

This section provides additional details to support our theoretical and empirical results in the main text, including the cross-entropy loss function, principal component analysis, and the proof for the main theorem.

### 5.1. Cross-entropy loss function

The cross-entropy (CE) loss function quantifies the discrepancy between predicted and actual probability distributions in classification tasks. As a standard metric, it guides model optimization through gradient descent. In this study, we employ CE loss to evaluate the empirical performance of Pre+TTN-VQC, TTN-VQC, and VQC models.

### 5.2. Principal Component Analysis

Principal component analysis (PCA) [40, 41] is a dimensionality reduction technique to transform high-dimensional data into a lower-dimensional space while preserving the most significant information. PCA effectively reduces feature space by identifying principal components that capture the maximum variance in the data. In this work, we employ PCA to map high-dimensional classical data onto a lower-dimensional space aligned with the qubit count of the VQC.

### 5.3. Proof of theoretical results

The section presents the proof of our derived theoretical results on the transfer learning risk. To begin with, we first introduce the conditions in Assumption 1 that ensure the following theorems.

**Assumption 1 (Regularity conditions)** *The following regularity conditions hold:*

- *The loss function  $\ell(\cdot, \cdot)$  is  $B$ -bounded, and  $\ell(\cdot, y)$  is  $L$ -Lipschitz for all  $y \in \mathcal{Y}$ .*
- *$\forall f \in \mathbb{F}$ , the function  $f$  is  $L(\mathbb{F})$ -Lipschitz with respect to the  $l_2$ -norm distance.*
- *Given a scalar constant  $D_S$ , if a composition function  $f \circ h$  is bounded, where  $\forall f \in \mathbb{F}, h \in \mathbb{H}$ , we have  $\sup_{\mathbf{x} \in S} |f \circ h(\mathbf{x})| \leq D_S$ .*

Then, we present the metric of representation difference  $d_{\mathbb{F}, f}(h', h)$  that captures the extent that  $h$  and  $h'$  differ in terms of their training losses, as shown in Definition 1.

**Definition 1** *For a functional class  $\mathbb{F}$ ,  $\forall f \in \mathbb{F}$  and an underlying distribution  $\mathcal{D}$  generating a sample  $(\mathbf{x}, y)$ , given a specific function  $f \in \mathbb{F}$ , the representation difference between two representations  $h, h' \in \mathbb{H}$  is given in Eq. (11).*

$$d_{\mathbb{F}, f}(h'; h) = \inf_{f' \in \mathbb{F}} \mathbf{E}_{(\mathbf{x}, y) \sim \mathcal{D}} [\ell(f' \circ h'(\mathbf{x}), y) - \ell(f \circ h(\mathbf{x}), y)]. \quad (11)$$

Moreover, given a dataset  $S$  with  $|S|$  samples, we consider an empirical Rademacher complexity over the functional class  $\mathbb{F}$  as shown in Eq. (12).

$$\hat{\mathcal{R}}_S(\mathbb{F}) = \mathbf{E}_{\sigma} \left[ \frac{1}{|S|} \sup_{f \in \mathbb{F}} \sum_{n=1}^{|S|} \sigma_n f(\mathbf{x}_n) \right], \quad (12)$$

where  $\sigma_n$  denotes a Rademacher random variable which takes values from  $-1$  to  $1$  with an equal probability. Then, for our proposed pre-trained methodology based on Pre+TTN-VQC, we can attain Theorem 1 as follows:

**Theorem 1** *Let  $\hat{f}_{\text{ttn}} \in \mathbb{F}_{\text{TTN}}$  be an empirical risk minimizer of TTN by minimizing  $\hat{R}_{\text{tr}}(\cdot, \cdot)$ . Then, if Assumption 1 holds, with a probability of at least  $1 - \delta$ , Eq. (13) stands.*

$$\begin{aligned} d_{\mathbb{F}_A, f_a}(\hat{f}_{\text{ttn}}; f_{\text{ttn}}^*) &\leq 16L\hat{\mathcal{R}}_S(\mathbb{F}_{\text{TTN}} \cup \mathbb{F}_A) + 8B\sqrt{\frac{\log(2/\delta)}{|S_0|}} \\ &\leq 16L\sqrt{\frac{\mathcal{C}(\mathbb{F}_{\text{TTN}} \cup \mathbb{F}_A)}{|S_0|}} + 8B\sqrt{\frac{\log(2/\delta)}{|S_0|}} \\ &\leq 16L\sqrt{\frac{\mathcal{C}(\mathbb{F}_{\text{TTN}}) + \mathcal{C}(\mathbb{F}_A)}{|S_0|}} + 8B\sqrt{\frac{\log(2/\delta)}{|S_0|}}, \end{aligned} \quad (13)$$

where  $\mathcal{C}(\mathbb{F}_{\text{TTN}})$  and  $\mathcal{C}(\mathbb{F}_A)$  capture the dimension-dependent size of the functional classes.

Since Definition 1 focuses on a specific function  $f \in \mathbb{F}$ , we can consider the worst-case representation difference as shown in Definition 2.

**Definition 2** *For a functional class  $\mathbb{F}$  such that  $f' \in \mathbb{F}$ ,  $f \in \mathbb{F}$ , and a sample  $(\mathbf{x}, y) \sim \mathbb{P}$ , the worst-case representation difference between representations  $h, h' \in \mathbb{H}$  is given in Eq. (14).*

$$d_{\mathbb{F}, \mathbb{F}}(h'; h) = \sup_{f' \in \mathbb{F}} \mathbf{E}_{(\mathbf{x}, y) \sim \mathbb{P}} [\ell(f' \circ h'(\mathbf{x}), y) - \ell(f \circ h(\mathbf{x}), y)]. \quad (14)$$

For a constant  $\nu$  related to the task-agnostic notion of task diversity, the worst-case representation difference in Definition 2 can be connected to Definition 1 as given in Eq. (15).

$$d_{\mathbb{F}, \mathbb{F}}(h'; h) \leq \frac{d_{\mathbb{F}, f}(h'; h)}{\nu} + \epsilon. \quad (15)$$

Then, we introduce Theorem 2 that is related to the transfer learning risk, as follows:

**Theorem 2** *Let  $\hat{f}_{\text{vqc}} \in \mathbb{F}_{\text{VQC}}$  be an empirical risk minimizer of VQC by minimizing  $\hat{R}_{\text{tr2}}(\cdot, \hat{f}_{\text{ttn}})$  for a pre-trained TTN  $\hat{f}_{\text{ttn}} \in \mathbb{F}_{\text{TTN}}$ . Then, if Assumption 1 holds, let  $f_{\text{vqc}}^* \in \mathbb{F}_{\text{VQC}}$  and  $f_{\text{ttn}}^* \in \mathbb{F}_{\text{TTN}}$  be optimal VQC and TTN, respectively, with a probability of at least  $1 - \delta$ , Eq. (16) stands.*

$$\begin{aligned}
R_{\text{tl}} &= R_{\text{tr2}}(\hat{f}_{\text{vqc}}, \hat{f}_{\text{ttn}}) - R_{\text{tr2}}(f_{\text{vqc}}^*, f_{\text{ttn}}^*) \\
&= \frac{1}{M} \sum_{m=1}^M \ell(\hat{f}_{\text{vqc}} \circ \hat{f}_{\text{ttn}}(\mathbf{x}_m), y_m) - \ell(f_{\text{vqc}}^* \circ f_{\text{ttn}}^*(\mathbf{x}_m), y_m) \\
&= \frac{1}{M} \sum_{m=1}^M \ell(\hat{f}_{\text{vqc}} \circ \hat{f}_{\text{ttn}}(\mathbf{x}_m), y_m) - \ell(\hat{f}_{\text{vqc}} \circ f_{\text{ttn}}^*(\mathbf{x}_m), y_m) \\
&\quad + \ell(\hat{f}_{\text{vqc}} \circ f_{\text{ttn}}^*(\mathbf{x}_m), y_m) - \ell(f_{\text{vqc}}^* \circ f_{\text{ttn}}^*(\mathbf{x}_m), y_m) \tag{16} \\
&\leq d_{\mathbb{F}_{\text{VQC}}, \mathbb{F}_{\text{VQC}}}(\hat{f}_{\text{ttn}}, f_{\text{ttn}}^*) + d_{\mathbb{F}_{\text{VQC}}, f_{\text{vqc}}}(\hat{f}_{\text{ttn}}, f_{\text{ttn}}^*) \\
&\leq d_{\mathbb{F}_{\text{A}}, \mathbb{F}_{\text{A}}}(\hat{f}_{\text{ttn}}, f_{\text{ttn}}^*) + 16L\hat{\mathcal{R}}_{S_T}(\mathbb{F}_{\text{VQC}}) + 8B\sqrt{\frac{\log(2/\delta)}{|S_T|}} \\
&\leq \frac{1}{\nu} d_{\mathbb{F}_{\text{A}}, f_{\text{A}}}(\hat{f}_{\text{ttn}}, f_{\text{ttn}}^*) + 16L\hat{\mathcal{R}}_{S_T}(\mathbb{F}_{\text{VQC}}) + \mathcal{O}(1),
\end{aligned}$$

where  $\hat{\mathcal{R}}_{S_T}(\mathbb{F}_{\text{VQC}}) \sim \sqrt{\frac{\mathcal{C}(\mathbb{F}_{\text{VQC}})}{|S_T|}}$ , and the target dataset  $S_T$  contains  $|S_T|$  samples. Here,  $\mathcal{C}(\mathbb{F}_{\text{VQC}})$  is related to the dimension-dependent size of the functional class.

By combining the results of Theorem 1 and Theorem 2, we can prove the transfer learning risk of Pre+TTN-VQC as given in Eq. (17).

$$R_{\text{tl}} = \tilde{\mathcal{O}} \left( \frac{1}{\nu} \left( \sqrt{\frac{\mathcal{C}(\mathbb{F}_{\text{TTN}}) + \mathcal{C}(\mathbb{F}_{\text{A}})}{|S_0|}} \right) + \sqrt{\frac{\mathcal{C}(\mathbb{F}_{\text{VQC}})}{|S_T|}} \right) \tag{17}$$

## 6. DATA AVAILABILITY

The dataset in our experiments of semiconductor quantum dot classification can be accessed via the website: [https://gitlab.com/QMAI/mlqe\\_2023\\_edx](https://gitlab.com/QMAI/mlqe_2023_edx), and the MNIST dataset can be downloaded via <http://yann.lecun.com/exdb/mnist>.

## 7. CODE AVAILABILITY

Our codes for implementing Pre+TTN-VQC, TTN-VQC, and VQC can be accessed at <https://github.com/uwjunqi/Pretrained-TTN-VQC>.

## 8. REFERENCE

- [1] Yunchao Liu, Srinivasan Arunachalam, and Kristan Temme, “A Rigorous and Robust Quantum Speed-up in Supervised Machine Learning,” *Nature Physics*, vol. 17, no. 9, pp. 1013–1017, 2021.
- [2] M Cerezo, Guillaume Verdon, Hsin-Yuan Huang, Lukasz Cincio, and Patrick J Coles, “Challenges and Opportunities in Quantum Machine Learning,” *Nature Computational Science*, vol. 2, no. 9, pp. 567–576, 2022.
- [3] Matthias C Caro et al., “Generalization in Quantum Machine Learning From Few Training Data,” *Nature Communications*, vol. 13, no. 1, pp. 4919, 2022.

- [4] Brian Coyle, Daniel Mills, Vincent Danos, and Elham Kashefi, “The Born Supremacy: Quantum Advantage and Training of An Ising Born Machine,” *npj Quantum Information*, vol. 6, no. 1, pp. 1–11, 2020.
- [5] Jacob Biamonte, Peter Wittek, Nicola Pancotti, Patrick Rebentrost, Nathan Wiebe, and Seth Lloyd, “Quantum Machine Learning,” *Nature*, vol. 549, no. 7671, pp. 195–202, 2017.
- [6] John Preskill, “Quantum Computing in the NISQ Era and Beyond,” *Quantum*, vol. 2, pp. 79, 2018.
- [7] Laird Egan et al., “Fault-tolerant Control of An Error-Corrected Qubit,” *Nature*, vol. 598, no. 7880, pp. 281–286, 2021.
- [8] Jun Qi and Min-Hsiu Hsieh, “Federated Quantum Natural Gradient Descent for Quantum Federated Learning,” in *Federated Learning*, pp. 329–341. Elsevier, 2024.
- [9] Hsin-Yuan Huang et al., “Power of Data in Quantum Machine Learning,” *Nature Communications*, vol. 12, no. 1, pp. 1–9, 2021.
- [10] Elisabet Romero, Ramunas Augulis, Vladimir I Novoderezhkin, Marco Ferretti, Jos Thieme, Donatas Zigmantas, and Rienk Van Grondelle, “Quantum Coherence in Photosynthesis for Efficient Solar-Energy Conversion,” *Nature Physics*, vol. 10, no. 9, pp. 676–682, 2014.
- [11] Abhinav Kandala, Antonio Mezzacapo, Kristan Temme, Maika Takita, Markus Brink, Jerry M Chow, and Jay M Gambetta, “Hardware-Efficient Variational Quantum Eigensolver for Small Molecules and Quantum Magnets,” *Nature*, vol. 549, no. 7671, pp. 242–246, 2017.
- [12] Marco Cerezo et al., “Variational Quantum Algorithms,” *Nature Reviews Physics*, vol. 3, no. 9, pp. 625–644, 2021.
- [13] Kerstin Beer et al., “Training Deep Quantum Neural Networks,” *Nature Communications*, vol. 11, no. 1, pp. 808, 2020.
- [14] Iris Cong, Soonwon Choi, and Mikhail D Lukin, “Quantum Convolutional Neural Networks,” *Nature Physics*, vol. 15, no. 12, pp. 1273–1278, 2019.
- [15] Amira Abbas, David Sutter, Christa Zoufal, Aurélien Lucchi, Alessio Figalli, and Stefan Woerner, “The Power of Quantum Neural Networks,” *Nature Computational Science*, vol. 1, no. 6, pp. 403–409, 2021.
- [16] Christa Zoufal, Aurélien Lucchi, and Stefan Woerner, “Quantum Generative Adversarial Networks for Learning and Loading Random Distributions,” *npj Quantum Information*, vol. 5, no. 1, pp. 1–9, 2019.
- [17] Yuxuan Du, Min-Hsiu Hsieh, Tongliang Liu, Shan You, and Dacheng Tao, “Learnability of Quantum Neural Networks,” *PRX Quantum*, vol. 2, no. 4, pp. 040337, 2021.
- [18] James Stokes, Josh Izaac, Nathan Killoran, and Giuseppe Carleo, “Quantum Natural Gradient,” *Quantum*, vol. 4, pp. 269, 2020.
- [19] Jarrod R McClean, Sergio Boixo, Vadim N Smelyanskiy, Ryan Babbush, and Hartmut Neven, “Barren Plateaus in Quantum Neural Network Training Landscapes,” *Nature Communications*, vol. 9, no. 1, pp. 1–6, 2018.
- [20] Jun Qi, Chao-Han Huck Yang, Pin-Yu Chen, and Min-Hsiu Hsieh, “Theoretical Error Performance Analysis for Variational Quantum Circuit Based Functional Regression,” *npj Quantum Information*, vol. 9, no. 1, pp. 4, 2023.
- [21] Ivan V Oseledets, “Tensor-Train Decomposition,” *SIAM Journal on Scientific Computing*, vol. 33, no. 5, pp. 2295–2317, 2011.
- [22] Jun Qi, Chao-Han Huck Yang, Pin-Yu Chen, and Javier Tejedor, “Exploiting Low-Rank Tensor-Train Deep Neural Networks Based on Riemannian Gradient Descent With Illustrations of Speech Processing,” *IEEE/ACM Transactions on Audio, Speech, and Language Processing*, vol. 31, pp. 633–642, 2023.
- [23] Samuel Yen-Chi Chen, Chih-Min Huang, Chia-Wei Hsing, and Ying-Jer Kao, “An End-to-End Trainable Hybrid Classical-Quantum Classifier,” *Machine Learning: Science and Technology*, vol. 2, no. 4, pp. 045021, 2021.
- [24] Hamed Karimi, Julie Nutini, and Mark Schmidt, “Linear Convergence of Gradient and Proximal-

- Gradient Methods Under the Polyak-Łojasiewicz Condition,” in *Joint European Conference on Machine Learning and Knowledge Discovery in Databases*. Springer, 2016, pp. 795–811.
- [25] Andrea Mari, Thomas R Bromley, Josh Izaac, Maria Schuld, and Nathan Killoran, “Transfer Learning in Hybrid Classical-Quantum Neural Networks,” *Quantum*, vol. 4, pp. 340, 2020.
- [26] Chao-Han Huck Yang, Jun Qi, Samuel Yen-Chi Chen, Yu Tsao, and Pin-Yu Chen, “When BERT Meets Quantum Temporal Convolution Learning for Text Classification in Heterogeneous Computing,” in *IEEE International Conference on Acoustics, Speech and Signal Processing*, 2022.
- [27] Jun Qi and Javier Tejedor, “Classical-to-Quantum Transfer Learning for Spoken Command Recognition Based on Quantum Neural Networks,” *IEEE International Conference on Acoustics, Speech and Signal Processing*, 2021.
- [28] Arun James Thirunavukarasu et al., “Large Language Models in Medicine,” *Nature Medicine*, vol. 29, no. 8, pp. 1930–1940, 2023.
- [29] Renqian Luo, Lai Sun, Yingce Xia, Tao Qin, Sheng Zhang, Hoifung Poon, and Tie-Yan Liu, “BioGPT: Generative Pre-trained Transformer for Biomedical Text Generation and Mining,” *Briefings in Bioinformatics*, vol. 23, no. 6, pp. bbac409, 2022.
- [30] James Dborin, Fergus Barratt, Vinul Wimalaweera, Lewis Wright, and Andrew G Green, “Matrix Product State Pre-training for Quantum Machine Learning,” *Quantum Science and Technology*, vol. 7, no. 3, pp. 035014, 2022.
- [31] Karl Weiss, Taghi M Khoshgoftaar, and DingDing Wang, “A survey of Transfer Learning,” *Journal of Big data*, vol. 3, pp. 1–40, 2016.
- [32] Jun Qi, Chao-Han Yang, and Pin-Yu Chen, “QTN-VQC: An End-to-End Learning Framework for Quantum Neural Networks,” *Physica Scripta*, vol. 99, no. 1, pp. 015111, 2023.
- [33] Alexander Novikov, Dmitrii Podoprikhin, Anton Osokin, and Dmitry P Petrov, “Tensorizing Neural Networks,” in *Advances in Neural Information Processing Systems*, 2015, vol. 28.
- [34] Pieter-Tjerk De Boer, Dirk P Kroese, Shie Mannor, and Reuven Y Rubinstein, “A Tutorial on the Cross-Entropy Method,” *Annals of Operations Research*, vol. 134, pp. 19–67, 2005.
- [35] Michele Donini et al., “Empirical Risk Minimization under Fairness Constraints,” *Advances in Neural Information Processing Systems*, vol. 31, 2018.
- [36] Li Deng, “The MNIST Database of Handwritten Digit Images for Machine Learning Research,” *IEEE Signal Processing Magazine*, vol. 29, no. 6, pp. 141–142, 2012.
- [37] S De Rinaldis et al., “Intrinsic Exciton-exciton Coupling in GaN-based Quantum Dots: Application to Solid-state Quantum Computing,” *Physical Review B*, vol. 65, no. 8, pp. 081309, 2002.
- [38] Joshua Ziegler et al., “Tuning Arrays with Rays: Physics-informed Tuning of Quantum Dot Charge States,” *Physical Review Applied*, vol. 20, no. 3, pp. 034067, 2023.
- [39] Jana Darulová et al., “Autonomous Tuning and Charge-state Detection of Gate-defined Quantum Dots,” *Physical Review Applied*, vol. 13, no. 5, pp. 054005, 2020.
- [40] Michael Greenacre et al., “Principal Component Analysis,” *Nature Reviews Methods Primers*, vol. 2, no. 1, pp. 100, 2022.
- [41] Markus Ringnér, “What Is Principal Component Analysis?,” *Nature Biotechnology*, vol. 26, no. 3, pp. 303–304, 2008.

## 9. COMPETING INTERESTS

The authors declare no Competing Financial or Non-Financial Interests.